The stability under irradiation of hollandite ceramics, specific radioactive cesium-host wasteforms

V. Aubin-Chevaldonnet, F. Studer, Daniel Caurant, D. Gourier, N. Nguyen, A. Ducouret, N. Baffier, T. Advocat

The stability under irradiation of hollandite ceramics, specific radioactive cesium-host wasteforms

V. Aubin[(1)], F. Studer[(2)], D. Caurant[(1)], D. Gourier[(1)], N. Nguyen[(2)], A. Ducouret[(2)], N. Baffier[(1)], T. Advocat[(4)]

[(1)]*LCAES (UMR CNRS 7574), 11 rue P. et M. Curie, Paris, France, 75231*
[(2)]*CRISMAT/ISRMA, 6 boulevard Maréchal Juin, Caen, France, 14050*
[(3)] *CEA/DEN/DIEC/SCDV/LEBV, BP17171, Marcoule, Bagnols-sur-Cèze, France, 30207*
vaubin@ext.jussieu.fr

Abstract *– Investigations are currently performed on matrices for the specific immobilization of long-lived radionuclides such as fission products resulting from an enhanced reprocessing of spent fuel. Hollandite (nominally $BaAl_2Ti_6O_{16}$), one of the phases constituting Synroc, receives renewed interest as specific Cs-host wasteform. The radioactive cesium isotopes decay involves the emission of β particles, γ rays and the transmutation of Cs to stable Ba ions. This study deals with the synthesis of hollandite ceramics by oxide route and single crystals by a flux method having the $Ba_xCs_y(Al,Fe)_{2x+y}Ti_{8-2x-y}O_{16}$ composition type ($1 \le x \le 1.28$; $0 \le y \le 0.28$). The influence of the hollandite chemical composition on the hollandite structure and microstructure is studied. To estimate the hollandite radiation resistance, external electron irradiation experiments, simulating the β particles emitted by radioactive cesium, were carried on single phase materials. The radiation effects were characterized by electron paramagnetic resonance (EPR) and Mössbauer spectroscopy.*

INTRODUCTION

Over the past few years, progress on the enhanced reprocessing of nuclear spent fuel and notably on separating the long-lived fission products from the high level radioactive wastes (HLW) has encouraged the investigations on specific host matrices [1]. Particularly, the success of cesium extraction by calixarenes complexes, except for some traces of rubidium, suggests that new materials with higher performances than borosilicate glassy matrices currently used to immobilize unseparated HLW, could be considered.

Cesium appears as one of the most hazardous radionuclide to immobilize because of the high thermal power of ^{134}Cs and ^{137}Cs isotopes, the long lifetime of ^{135}Cs isotope ($T_{1/2}$=2,3 10^6 years), its volatility at high temperature during waste forms synthesis and its tendency to form water-soluble compounds. The cesium radioactive isotopes decay into stable barium by emitting β particles (with energy E ranging from 0.09 to 1.17 MeV, mainly 0.5 MeV) and γ rays (E≈0.6 MeV). Therefore, the choice of new Cs-host matrices rely on their waste (Cs, Rb) loading, their Ba and Sr (decay product of Rb) incorporation ability, their thermal characteristics, their long-term containment properties (chemical durability, βγ radiation resistance) and the ease of their synthesis.

Among several Cs-specific matrices proposed (refractory aluminosilicate glasses [2], zeolites [3], pollucite ceramics [4]), hollandite of $[Ba^{2+}_xCs^{+}_y][(Al^{3+},Ti^{3+})_{2x+y}\ Ti^{4+}_{8-2x-y}]O_{16}$ (x+y<2) composition, widely studied within the framework of Synroc - a multiphase assemblage of ceramics developed for the immobilization of unseparated HLW - remains one of the best Cs-host matrice.

The hollandite type $A_2B_8O_{16}$ structure (A=Ba, Cs and B=Al,Ti), shown in Fig. 1, is closely related to the rutile structure. It is tetragonal (I4/m space group) or monoclinic (I2/m) according to the ionic radii of A and B cations. The $[BO_6]$ octahedra are linked by edges and corners to form one-dimensional square tunnels in which are located the large A cations. The tunnel sites are often not full and depending on the hollandite

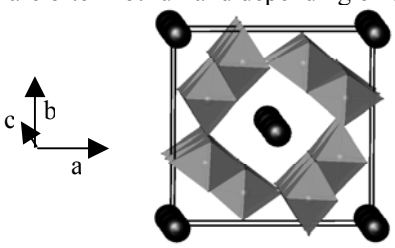

Fig. 1. View of the tetragonal (I4/m) hollandite-type $A_2B_8O_{16}$ structure approximately along the c-axis: A cations (black atoms) and $[TiO_6]$ octahedra are shown .

composition, the A cations and vacant sites may take up an ordered arrangement along the tunnels (superlattice ordering).
Hollandite has several advantages. It is able to accommodate chemistry and valence changes due to the cesium transmutation because of its high capacity to incorporate Ba in its structure and due to the possibility of reduction of a fraction of Ti^{4+} ions to ensure the charge balance [5]. Moreover, its chemical durability is two orders of magnitude higher than the currently used borosilicate glasses, which is required to select Cs-specific matrices [6]. Nevertheless, the synthesis of $[Ba^{2+}_xCs^{+}_y][(Al^{3+},Ti^{3+})_{2x+y}\ Ti^{4+}_{8-2x-y}]O_{16}$ composition, named afterwards the Synroc composition, remains actually too complex to be industrialized [7]. Indeed, its synthesis consists of a hot pressing stage under controlled redox conditions of a precursor obtained by an alkoxide route. The substitution of Ti^{3+} by Fe^{3+} in the Synroc composition enables to obtain single phase (Ba,Cs)-hollandite using a natural sintering under air of a precursors mixture prepared by an alkoxide route [8], which clearly simplifies the protocol. The next step is to use the oxide route to get these hollandite ceramics, which will be described in this study. On the other hand, the βγ radiation resistance of hollandite is not yet proved due to the lack of both true natural analogs and experiments on synthetic hollandite samples containing radioactive cesium. Moreover, literature reports only electron external irradiation experiments which overestimate the real effects of β irradiation. Indeed, only experiments under intense electron irradiation in electron microscope were carried out on single phase hollandite, which generated microtwinnings followed by amorphization [9]. Other external irradiations were performed on hollandite samples, simulating the α irradiation which could come from the α-emitting surrounding actinide-contaning phases (such as in Synroc assemblage) [10]. However, these radiation effects are not to be considered in the case of Cs-specific immobilization and can not be extrapolated to predict the hollandite βγ-radiation resistance.
In this work, we report the synthesis of hollandite ceramics in the $Ba_xCs_y(Al,Fe)_{2x+y}Ti_{8-2x-y}O_{16}$ formula range by an oxide route and their microstructure. Among the different compositions studied, the most simple formulae (y=0) were selected for external electron irradiation experiments and then characterized by electron paramagnetic resonance (EPR) and/or Mössbauer spectroscopy. Hollandite single crystals were also prepared to get more precise informations about the irradiation-induced point defects detected by EPR.

EXPERIMENTAL

Several ceramics having the $Ba^{2+}_xCs^{+}_y(C=Al,Fe)^{3+}_{2x+y}Ti^{4+}_{8-2x-y}O_{16}$ composition type ($1\leq x\leq 1.28$; $0\leq y\leq 0.28$) were prepared by solid-state reaction from Al_2O_3, Fe_2O_3, TiO_2, $BaCO_3$ and $CsNO_3$ in air. Iron is introduced in hollandite because it was reported to facilitate both the synthesis protocol (heat treatment under reducing atmosphere is avoided) [8] and the insertion of cesium in hollandite structure (increase of channels size) [7]. We study this composition range by varying the Al/Fe and Cs/Ba ratios (Table I).
The reagent powders (almost 30g) were mixed, ground in an agate mortar, pelletized and calcined under air for 4 hours at 810°C. The calcined powder was then ground with an attrition mill with zirconia-based glass-ceramics or yttria zirconia (indicated with * near the composition sample in Table I) balls in water for 1 hour at 550 rpm (rounds per minute). This fine grinding stage is absolutely necessary to synthesize (Ba, Cs)-hollandite because it increases the precursor homogeneity and reactivity and so decreases both sintering temperature and duration. Once the precursor dried (at 100°C for 1-2 days), it was pelletized and sintered at 1200°C for 30 hours under air. The optimization of this synthesis was already reported in [11].
Samples were characterized by X-ray diffraction (XRD) with CoKα wavelength (λ= 1.78897 Å), by Scanning Electron Microscopy (SEM), Energy Dispersive X-ray Analysis (EDX) and by Electron Probe MicroAnalysis (EPMA). For enough densified samples, the ceramic density d was deduced from the Archimede force applied in toluene solvent and was then compared to the theoretical density d_{th} deduced from the lattice parameters extracted from XRD patterns.
Hollandite single crystals of the most simple composition $Ba_{1.16}Al_{2.32}Ti_{5.68}O_{16}$ were also synthesized by a flux method. The choice of the crystal growth method results from the incongruent melting of hollandite (as verified for the $Ba_{1.16}Al_{2.32}Ti_{5.68}O_{16}$ composition by both differential thermal analysis experiments and slow cooling from the melt). This new synthesis protocol is precisely described in [12]: flux (47% mol. BaF_2 - 53% mol B_2O_3) added to hollandite

ceramic powder at 40% wt. This mixture was melted at 1400°C and then slowly cooled to room temperature (3 to 12°C/h).

TABLE I. theoretical and EPMA compositions of hollandite ceramics.

	Expected compositions	EPMA compositions
1	$Ba_{1.16}Al_{2.32}Ti_{5.68}O_{16}$	$Ba_{1.18}Al_{2.28}Ti_{5.69}O_{16}$
2	$Cs_{0.1}Ba_{1.11}Al_{2.32}Ti_{5.68}O_{16}$	$Cs_{0.05}Ba_{1.17}Al_{2.30}Ti_{5.67}O_{16}$
3	$Ba_{1.28}Al_{1.64}$ $Fe_{0.92}Ti_{5.44}O_{16}$	$Ba_{1.29}Al_{1.71}Fe_{0.93}Ti_{5.38}O_{16}$
4	$Cs_{0.28}Ba_{1}Al_{1.46}Fe_{0.82}Ti_{5.72}O_{16}$	$Cs_{0.25}Ba_{1.05}Al_{1.43}Fe_{0.80}Ti_{5.74}O_{16}$
5	$Ba_{1.16}Fe_{2.32}Ti_{5.68}O_{16}$	$Ba_{1.13}Fe_{2.32}Ti_{5.70}O_{16}$
6	$^{*}Cs_{0.24}Ba_{1.04}Fe_{2.32}Ti_{5.68}O_{16}$	$Cs_{0.26}Ba_{1.06}Fe_{2.28}Ti_{5.70}O_{16}$

End-member Ba-hollandite (y=0) materials were irradiated by 1, 1.5 or 2.5 MeV electrons generated by a Van de Graaff accelerator to simulate the effect of β particles emitted by radioactive cesium. The thickness of samples (0.5 or 1 mm) was chosen so that electrons go through the sample and radiations effects are quite homogeneous. Different fluences between $8.1\ 10^{17}$ and $1.4\ 10^{19}$ cm^{-2} were carried out. As electron irradiations generate mainly electron excitations of materials and few atomic displacements, the techniques used to characterize the radiation effects were sensitive local spectroscopies: EPR , Mössbauer spectroscopy, depending on samples composition.

The ^{57}Fe transmission Mössbauer spectra were measured at room temperature using a $^{57}CoRh$ source on Fe-rich powders or thin massive samples. The isomer shift (I.S.) are corrected for the I.S. of metallic iron taken as a reference. The spectra were simulated thanks to a least square fitting routine assuming a Lorentzian line shape. The EPR spectra were recorded on a Bruker ESP 300e or an ELEXYS E500 spectrometer operating at X band (9.4 GHz) in the range of temperature 6-300K. The EPR signals were simulated using the software SIMFONIA. The spin concentration associated with EPR signals was determined by comparison with the organic radical standard DPPH. The main study was performed on Ba-Al hollandite (C=Al) because the occurence of Fe^{3+} (paramagnetic $3d^5$ ion) induced a strong and wide contribution on EPR spectra that could prevent the detection of irradiation-induced defects.

RESULTS AND DISCUSSION

XRD and SEM Characterizations of Hollandite Ceramics

The hollandite ceramics with C=Al (samples 1 and 2) were first synthesized using the protocol described above. The Ba-Al-hollandite was obtained as single phase and was relatively dense (d/d_{th}=95%, Fig. 2a.). Its crystal structure is I4/m with the cell parameters indicated in Table II.

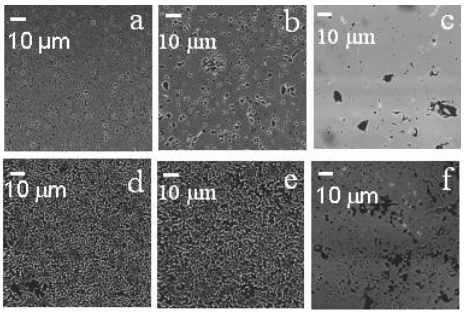

Fig. 2. Backscattered electron SEM micrographs of Ba-hollandite 1 (a), 3 (b), 5(c) and (Cs,Ba)-hollandite 2 (d), 4 (e), 6 (f) showing notably the difference of porosity (darken areas) between samples (all the samples were prepared following the same method).

TABLE II. Polyphased character of the hollandite ceramics. Lattice parameters a, c and unit-cell volume V (space group I4/m) are given for almost single phase samples.

	Secondary phases (XRD and SEM)	Lattice parameters		
		a (Å)	c (Å)	V ($Å^3$)
1	-	9.968	2.923	290.5
2	Al_2O_3,TiO_2,$Ba_2Ti_9O_{20}$	-	-	-
3	Impurities phase (traces)	10.003	2.944	294.5
4	-	10.042	2.942	296.7
5	Impurities phase (traces)	10.103	2.971	303.2
6	Fe_2TiO_5 (traces)	10.122	2.972	304.5

Then, we attempted to insert 0.1% Cs/formula unit, keeping constant the cations in octahedral sites. This Cs-content was chosen relatively low because literature indicates an upper limit of 0.25% Cs/formula unit for these type of hollandite ceramics prepared under air [13]. Nevertheless, this material was multiphase (Table II) and not densified (Fig.2d). EPMA (Table I) indicates that only half of cesium is incorporated in hollandite. Therefore, a fraction of Cs volatilized or was concentrated in a secondary phase not detected by SEM due to the high porosity of the material. The second hypothesis appears more probable because after a longer sintering treatment (96h), a Cs-rich secondary phase containing Al, Ti, Si cations (of too small size to be probed by EPMA to get its exact composition) was observed. We could

suppose that this phase is the well-known leachable $CsAlTiO_4$ phase already reported in literature [7] with a partial substitution of Ti by Si, by comparison with other synthesized materials not reported here. The occurrence of this phase seems to be due to kinetic factors which could be reduced by the partial substitution of Al^{3+} by bigger trivalent cations [7]. Moreover, this phase could be favored by the presence of Si impurities which originate in part from the TiO_2 raw material and from the attrition balls constituted of zirconia-based glass-ceramics.

To facilitate Cs incorporation in hollandite structure, Al^{3+} was substituted partially or totally by Fe^{3+}. The BaFe-hollandite (samples 3 and 5) are almost single phase except for a small white (backscattered electrons) phase enriched in Ba, P and Si only detected by SEM. This parasitical phase has been almost avoided afterwards by using very pure rutile as raw material. This impurities issue was already reported in [14]. These two ceramics were relatively dense (d/d_{th}=92,7% and 96% for the samples 3 and 5, respectively). By comparing their microstructures (Fig. 2.b and c), Al ions do not appear as a sintering reagent because the amount of porosities decreases when the Al/Fe ratio decreases. This Al-Fe substitution leads also to an increase of the lattice parameters a, c and of the unit-cell volume V (Table II), which is explained by the difference of ionic radii of Al^{3+} (r=0.535 Å) and Fe^{3+} (r=0.645 Å) [15]. Thus, a better insertion of Cs is expected in hollandite containing iron. Two different Cs contents (0.28 and 0.24/unit-cell Cs for samples 4 and 6 respectively) were incorporated because we want to synthesize exactly the $Cs_{0.28}Ba_1Al_{1.46}Fe_{0.82}Ti_{5.72}O_{16}$ composition reported in [8] to compare directly the alkoxide and oxide routes. Sample 4 is a single phase material with a composition very close to the expected one (4.45 wt% Cs_2O versus 5 wt% initially introduced, Table I). Unfortunately, this material has a high porosity as observed by SEM (Fig. 2e). Comparison with the BaFe-hollandite (Fig. 2b) microstructure shows that cesium prevents also a good densification of the ceramic. Sample 6 retains the entire cesium initially introduced (Table I) and is dense. However, traces of Fe_2TiO_5 and $BaTi_4O_9$ could be suspected by XRD (only 1-2 peaks), which does not raise issue because this secondary phase does not concentrate cesium. Increasing the time sintering would improve the material homogeneity. The densification of this ceramic is better than the sample 4 one (Fig.2e,f), which confirms that Al ions do not favor material densification. As shown by the lattice parameters of samples 3, 4, 5 and 6 (Table II), the incorporation of Cs induced an increase of a and V due to the large size of this cation, without changing c parameter.

Therefore, single phase (Ba,Cs)-hollandite ceramics could be synthesized by oxide route using natural sintering under air with a total retention of the cesium initially introduced. The best composition currently synthesized seems to be $Cs_{0.24}Ba_{1.04}Fe_{2.32}Ti_{5.68}O_{16}$ in terms of microstructure (lowest porosity). Moreover, replacing entirely Al^{3+} ions obviously reduces the amount of raw materials and avoids also the formation of the leachable $CsAlTiO_4$ phase. Thus, if Al ions do not influence the hollandite chemical durability, it appears useless to introduce these trivalent ions. The first measurements on the sample 6, currently in progress, tend to show that its chemical durability is as good as the hollandite ceramic reported in [8] and so that Al ions does not take part in the hollandite high chemical durability. Therefore, the $Cs_{0.24}Ba_{1.04}Fe_{2.32}Ti_{5.68}O_{16}$ hollandite composition is actually selected for this oxide synthesis.

Electron Irradiation Effects

Mössbauer Study

The sample 5 of composition $Ba_{1.16}Fe_{2.32}Ti_{5.68}O_{16}$ was selected in this study because no ^{57}Fe-enrichment was necessary and this composition is relatively simple with only one trivalent specie (Fe^{3+}) and one tunnel cation (Ba^{2+}). Its 300K Mössbauer spectrum (Fig. 3a) exhibits one quadrupolar doublet before irradiation. However, in order to obtain the best fit, it was necessary to consider two Mössbauer components whose parameters are indicated in Table III. Their isomer shift IS values (0.49 mm/s) are typical of Fe^{3+} ions. Only the quadrupole splitting (QS) differentiate these two sites. It agrees well with the iron octahedral environment with a more important distortion for site 1. Therefore, no Fe^{2+} ions are detected before irradiation.

In the tetragonal hollandite structure (I4/m space group), all the octahedral sites are equivalent and Fe^{3+} and Ti^{4+} ions are assumed to be randomized in them in the scale of the X-ray diffraction [16]. On the other hand, if the structure is monoclinic (I2/m space group), two crystallographic sites occur but without preferential occupation [16].

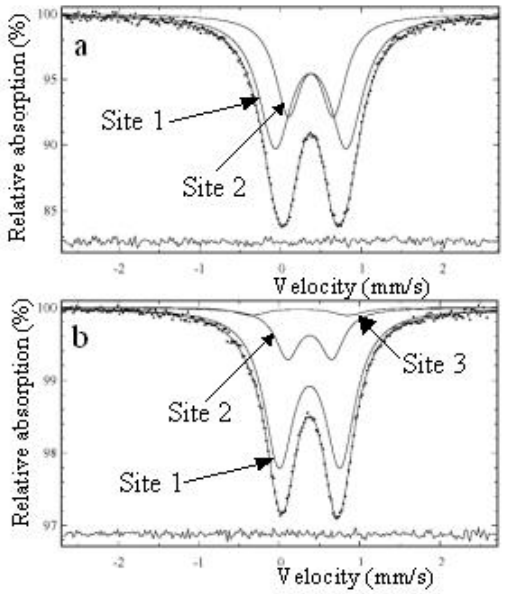

Fig. 3.Typical 300K Mössbauer spectra of sample 5 ($Ba_{1.16}Fe_{2.32}Ti_{5.68}O_{16}$) before (a) and after irradiation (b) with 1.5 MeV electrons at a fluence F 5.8 10^{18} cm^{-2}. The components used to simulate the experimental spectra are indicated by solid lines. The difference between the experimental and simulated spectra are shown below each spectrum.

However, few works are reported about local spectroscopies such as NMR, EPR and Mössbauer spectrocopies. Nevertheless, two Mössbauer studies on $K_{1.45}Fe_{1.45}Ti_{6.55}O_{16}$ [17]and $Cs_{1.40}Fe_{1.40}Ti_{6.74}O_{16}$ [18] hollandites report also one quadrupolar doublet at 300K whose parameters seem to be closer to the sample 5 site 2 ones. Moreover, literature reports a monoclinic structure for a close hollandite composition $Ba_{1.14}Fe_{2.28}Ti_{5.72}O_{16}$ [14]. Therefore, we can wonder whether our material does not display a slight monoclinic distortion not clearly detected by XRD and thus these two doublets (Fig. 3a) would be related to the two different crystallographic sites. This hypothesis is rejected by comparison with Mössbauer spectra of the samples 3 and 4 (I4/m space group) which display also 2 quadrupolar doublets, not shown here [19]. The crystal structure of these samples was confirmed by structural determination on single crystals of the same composition [12]. Therefore, only one crystallographic site is assumed for sample 5 and then these two different doublets could be assigned to different local environments of Fe^{3+} ions. First, this difference could be due to the possibility to have Fe^{3+} ions or Ti^{4+} ions as nearest neighbors. This explanation does not seem to be probable given the supposed random distribution of the Fe and Ti ions in the octahedral sites and the presence of only two quadrupolar doublets in samples 3 and 4 containing in addition Al ions [19]. Therefore, the occurrence of these two sites could only be explained by the occupancy of cation site in the tunnels. Indeed, this occupancy is not full and thus Fe^{3+} ions could have vacancies or Ba cations in their close environment (Fig.1). Moreover, it is known that B cations (Fe^{3+} notably) change their position in their octahedral site according to the local tunnel content [20], which could explain the different quadrupolar splitting of the two sites. This hypothesis is confirmed by the changes of the site fraction R with the hollandite chemical composition [19]. The exact environment of each site is nevertheless not yet fully determined.

TABLE III. Hyperfine parameters extracted from the least-squares fits of the 300K ^{57}Fe spectra of the pristine and electron irradiated sample 5 shown in Fig.3: Isomer shift (I.S.), quadrupole splitting (Q.S.), full width at half maximum (Γ) and fraction (R) of the different sites.

sample	sites	I.S mm/s.	Q.S. mm/s	Γ mm/s	R %
Pristine sample 5	1	0.493	0.884	0.25	63
	2	0.494	0.56	0.19	37
Irradiated sample 5	1	0.490	0.76	0.23	77
	2	0.492	0.55	0.12	19
	3	0.36	1.21	0.23	4

Although 300K experimental Mössbauer spectrum of the electron irradiated sample 5 exhibits only one quadrupolar doublet (Fig.3b), 3 iron components are necessary to reproduce it. The two first sites correspond to those observed before irradiation as shown by their associated parameters in Table III. Nevertheless, their relative fraction change in favor of the site 1 which becomes also more symmetric. This suggests that this irradiation modify the local arrangement of Ba cations around Fe^{3+} ions by atomic displacements of Ba ions. Moreover, a third site was generated in small quantities. Its smaller isomer shift and higher quadrupole splitting values, with respect to the two first sites, are more typical of a fivefold coordinated pyramidal Fe^{3+} ions. Therefore, this electron irradiation generates also some oxygen displacements. Finally, no change of the iron oxidation seems to occur: no Fe^{2+} ions were detected within the Mössbauer sensitivity scale.

Briefly, Mössbauer results show that this electron irradiation (E=1.5 MeV, F=5.8 10^{18} cm^{-2}) seems to generate atomic displacements of at least Ba and O ions without reduction of a significant fraction of the Fe^{3+} ions.

EPR study

The EPR study was carried out on ceramics and single crystals of the $Ba_{1.16}Al_{2.32}Ti_{5.68}O_{16}$ composition to avoid any interference between the irradiation-induced defects and Fe^{3+} ions (paramagnetic species).
Fig. 4 exhibits the typical EPR spectra of pristine and β-irradiated ceramics as a function of fluence and energy of electrons. The EPR spectra of irradiated samples display three new signals T_r, E_1 and E_2 whose intensities increase with increasing fluence without saturation up to 1.4 10^{19} cm^{-2} for 1 MeV electron irradiations. Their relative proportions depend not only on fluence but also on electron energy. Indeed, at almost the same fluence (5. 10^{18} cm^{-2}), the E_2 signal dominates the spectrum of the 2.5 and 1.5 MeV irradiated samples whereas it is weak for the sample irradiated by 1 MeV electrons. This influence of the electron energy suggests an effect of energy displacement threshold and obviously a mechanism of ballistic collisions associated with this signal E_2.

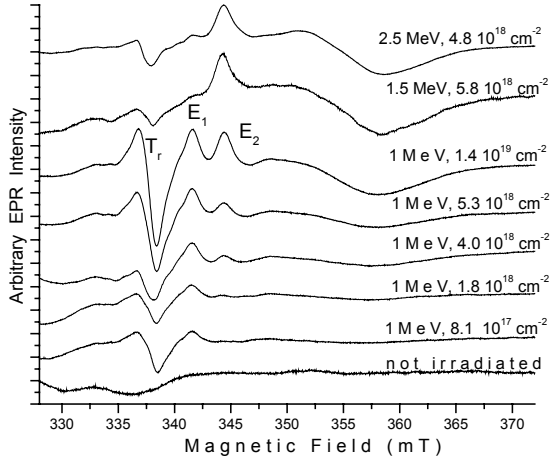

Fig. 4. Typical EPR spectra of $Ba_{1.16}Al_{2.32}Ti_{5.68}O_{16}$ hollandite before and after electron irradiation recorded at 70K with microwave power P =20 mW and microwave frequency ν =9.5 GHz. Energy of electrons and fluences are indicated near the spectra.

In order to attribute and quantify these signals, experimental spectra, recorded at different temperatures, were simulated [21]. The g-tensor and the linewidth associated to each signal are indicated in Table IV. Thus, two types of signals could be differentiated:

- The T_r signal , located near 337 mT corresponding to g-factor larger than the free electron g-factor (g_e=2.0023). Its position imply that the associated defects are hole centers. This signal is simulated considering the contribution of three orthorhombic sites differing only from the g_z value (Table IV) to account for the shoulders on the left-hand side of the signal. The computed g-factors are typical of oxygen species [22]. However, this signal cannot be assigned to a O^- center but rather to a superoxide ion O_2^- according to its g-shift sequence $g_{//} = g_z > g_\perp = 1/2(g_x+g_y) > g_e$. The associated spin concentration is in the range 4.2 10^{15}-5.4 10^{16} cm^{-3} when the fluence of 1 MeV electron is increased from 8.1 10^{17} to 1.4 10^{19} cm^{-2}.

Table IV. g-factors (g_x, g_y and g_z components) and corresponding half-width at half-maximum (ΔB mT) determined by the simulation of the three signals detected in ceramics after electron irradiation. All simulations were performed using gaussian shape lines. Two possible simulations of signal E_2 were found.

	g_x (ΔB_x)	g_y (ΔB_y)	g_z (ΔB_z)
Signal T_r	2.0038 (1.2) 2.0038 (1.2) 2.0038 (1.2)	2.009 (0.8) 2.009 (0.8) 2.009 (0.8)	2.035 (0.9) 2.026 (0.9) 2.018 (0.9)
Signal E_1	1.953 (3)	1.972 (3)	1.981 (1.5)
Signal E_2 (a)	1.885 (5.4)	1.912 (5.8)	1.966 (1.7)
Signal E_2 (b)	1.898 (7)	1.898 (7)	1.965 (1.5)

- The E_1 and E_2 signals, located near 341 and 344 mT (Fig.4), are characterized by g-factors (Table IV) smaller than g_e, which indicates that the corresponding defects are electron centers. Moreover, the g values are typical of Ti^{3+} ions in orthorhombic or axial sites [23]. The difference of lineshape between E_1 and E_2 signals could be explained by different local environments around Ti^{3+} ions. Moreover, these two signals are not similar to the native signals of Ti^{3+} ions in hollandite prior to irradiation [21], resulting from the partial reduction of titanium during the sintering. Therefore, the local environment of these Ti^{3+} ions was modified by electron irradiations. As E_1 and E_2 signals were observed in the temperature range

4-298K and 10-170K respectively, considerations about energy levels diagram (d orbitals) indicate that the Ti^{3+} ions responsible for E_2 signal are located in a less distorted site than Ti^{3+} ions associated with E_1 signal. However, the lineshape of E_2 signal is very atypical for titanium centers [Fig. 5a]. Their exact environment is not yet well determined. The spin concentration of Ti^{3+} ions responsible for $E_1$and E_2 signals are in the range 2.9 10^{15}-1.5.10^{16} and 1.8 10^{16}-2.3 10^{17} spins/cm^3 respectively when the samples were irradiated by 1 MeV electrons at a fluence ranging from 8.1 10^{17} to 1.4 10^{19} cm^{-2}. Therefore, the sum of the electron center concentrations is always higher than the hole center concentration. This difference could be explained by the fact that hole centers result from the trapping of several holes or that diamagnetic hole centers (not detected by EPR) could be generated.

All these defects are stable at room temperature for at least 2 years. Their thermal evolution (323-1073 K) is reported in [21].

To get more precise information on the nature of the irradiation-induced defects, single crystals of the same composition as the ceramics ($Ba_{1.16}Al_{2.32}Ti_{5.68}O_{16}$) were also irradiated. First, to confirm that the same signals were generated in ceramics and single crystals, the EPR powder spectrum of several ground single crystals was compared to the ceramic one (Fig.5). This spectrum (Fig. 5b) displays also the three signals T_r, E_1 and E_2 with only small lineshape differences which could simply be explained by the lack of some crystallite orientations versus the external magnetic field in the ground crystal powder. Their relative intensities are also very similar for the two samples. Therefore, these 3 signals can be assigned to defects localized in the bulk of samples.

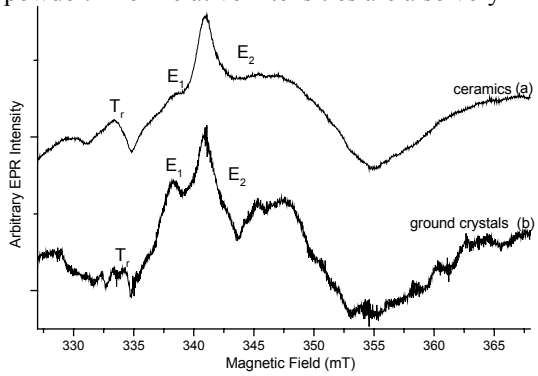

Fig. 5. Typical EPR spectra of $Ba_{1.16}Al_{2.32}Ti_{5.68}O_{16}$ ceramics (a) and ground crystals (b), both irradiated by 1.5 MeV at a fluence of 5.8 10^{18} cm^{-2}, recorded at 70K with P =20 mW and ν =9.4 GHz.

Unfortunately, only the signal E_2 could be entirely studied on single crystal because the two other signals were not strong enough to be detected (due to the small size of a single crystal). For this study, one single crystal whose growth axis and one face were determined by X-ray techniques as c axis and [110] type, was oriented such that the magnetic field of the EPR spectrometer lies in (110) and (001) planes. The EPR spectra display a single lorentzian signal at magnetic field B depending on the orientation of the crystal in each plane. Fig. 6 shows the angular dependence of g^2, with the factor $g = h\nu / \beta B$ with h the Planck constant, ν the microwave frequency, β the electron Bohr magneton. The very small amplitude of the angular variation, in the (001) plane, compared to that in the (110) plane, indicates that Ti^{3+} ions

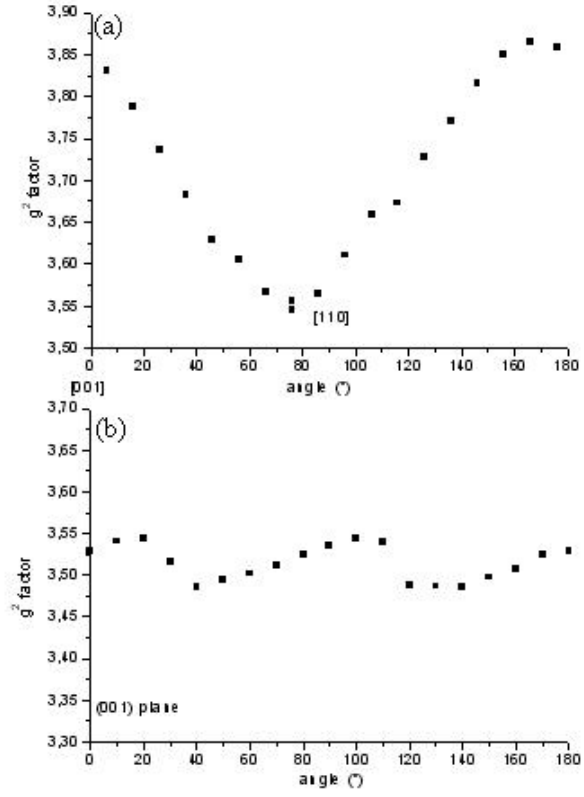

Fig. 6. Angular variations of the g^2 measured from the signal E_2 field position, observed on a $Ba_{1.16}Al_{2.32}Ti_{5.68}O_{16}$ single crystal irradiated by 1.5 MeV at a fluence of 5.8 10^{18} cm^{-2}, at 10K in (110) and (001) planes, (a) and (b) respectively.

occupy a site with quasi - axial symmetry . Thus, its variation in the plane (110) could be fitted by Eq.1 where Θ is the angle between the external magnetic field and the principal axis of g-tensor.

$$g^2=g_{//}^2\cos^2(\theta)+g_{\perp}^2\sin^2(\theta) \qquad (1)$$

The principal values $g_{\perp}$=1.8868, $g_{//}$=1.9646 are thus obtained, with z following the c axis. These g values agree well with one of the two possible simulations of the signal E_2 observed in ceramics (noted signal E_2 (b) in Table IV), which allows us to eliminate the other one. Moreover, these results show that the principal axis of the g-tensor follows the direction Ti-Ti along the $[TiO_6]$ octahedra chains. Moreover, this axial site symmetry is quite surprising given the important distortion of the octaedral sites . We can therefore wonder if this center would not be located in interstitial sites rather than in normal sites. In this latter case, it imply irradiation-induced titanium displacements.

CONCLUSIONS

Thus, single phase hollandite ceramics in the $Ba_xCs_y(C=Al,Fe)_{2x+y}Ti_{8-2x-y}O_{16}$ compositional range could be obtained by natural sintering under air of oxide powders only when iron is introduced. Nevertheless, the ceramic without Al seems to be the best one in terms of density and cesium retention. The behavior of several hollandite under external electron irradiation simulating the β-irradiation of radioactive cesium were also studied by EPR and Mössbauer spectroscopy. Both spectroscopies tend to show that atomics displacements of hollandite ions (O, Ba, B) could be generated, which modified the local environment of probed titanium and iron ions.

ACKNOWLEDGEMENTS

The authors are indebted to the DSM/DRECAM/LSI laboratory (Palaiseau, France) and particularly to Stéphane Esnouf for the runs at the Van de Graaff accelerator.

REFERENCES

1. C. MADIC, M. LECOMTE, P. BARON, B. BOULLIS, *C. R. Physique,* **3**, 797 (2002).
2. F. BART, S. SOUNILHAC, J. L. DUSSOSSOY, A. BONNETIER, C. FILLET, *Ceram. Trans*., **116**, 353 (2001).
3. D. P. STINTON, W. J. LACKEY, P. ANGELINI, *J. Am. Ceram. Soc,*. **66**, 389 (1983).
4. N. J. HESS, F. J. ESPINOSA, S. D. CONRADSON, W. J. WEBER, *J. Nucl. Mater.,* **281**, 22 (2000).
5. L. A. BURSILL, *J. Solid State Chem.,* **69**, 355 (1987).
6. M.L. CARTER, E.R. VANCE, D.R.G. MITCHELL, J.V. HANNA, Z. ZHANG, E. LOI, *J. Mater. Res*., **17**, 2578 (2002).
7. S.E. KESSON, *Radioact. Waste Manage. Nucl. Fuel Cycle* **4** (1), 53 (1983).
8. G. LETURCQ, F. BART, A. COMTE, patent n°E.N.01/15972 (december 2001).
9. L. A. BURSILL, D. J. SMITH, *J. Solid State Chem.*, **69**, 343 (1987).
10. W. J. WEBER, *Mat. Res. Soc. Symp. Proc.,* **44**, 671 (1985).
11. V. AUBIN, D. CAURANT, D. GOURIER, N. BAFFIER, T. ADVOCAT, F. BART, G. LETURCQ, J. M. COSTANTINI, Scientific Basis for Nuclear Waste Management XXVII, **807** (2004).
12. V. AUBIN, M. EVAIN, L. MAZEROLLES, A. Y. LEINEKUGEL-LE-COCQ, P. DENIARD, D. CAURANT, S. JOBIC, to be published.
13. R.W. CHEARY, J. KWIATKOWSKA, *J. Nucl. Mater.,* **125**, 236 (1984).
14. J.M. LOEZOS, T.A. VANDERAH, A.R. DREWS, *Powder diffraction,* **14** (1), 31 (1999).
15. R.D. SHANNON, *Acta. Cryst*., **A32**, 751 (1976).
16. R.W. CHEARY, *Acta. Cryst.,* **B42**, 229 (1986).
17. M. DROFENIK, D. HANZEL, *Mat. Res. Bull.,* **17**, 1457 (1982).
18. T. BIRCHALL, N.N. GREENWOOD, A.F. REID, *J. Chem. Soc.,* **A**, 2382 (1969).
19. V. AUBIN, F. STUDER, N. NGUYEN, A. DUCOURET, D. GOURIER, D. CAURANT, N. BAFFIER, *to be published*.
20. E. FANCHON, *thesis,* Université scientifique, technologique et medicale de Grenoble, (1987).
21. V. AUBIN, D. CAURANT, D. GOURIER, N. BAFFIER, S. ESNOUF, T. ADVOCAT, *Radiation Effects and Ion Beam Processing of Materials*, **792** (2004).
22. A.S. MARFUNIN, *Spectroscopy, luminescence and radiation centers in Minerals,* Springer-Verlag, New York, pp.257-262 (1979).
23. M. YAMAGA, T. YOSIDA, B. HENDERSON, K.P. O'DONNELL and M. DATE, *J. Phys. Condens. Matter.,* **4**, 7285 (1992).